

Phase equivalent potentials for three-body halos

E. Garrido

Instituto de Estructura de la Materia, CSIC,
Serrano 123, E-28006 Madrid, Spain

and

D.V. Fedorov and A.S. Jensen

Institute of Physics and Astronomy,
University of Aarhus, DK-8000 Aarhus C, Denmark

May 2, 2017

Abstract

We compare the properties of three-body systems obtained with two-body potentials with Pauli forbidden states and with the corresponding phase equivalent two-body potentials. In the first case the forbidden states are explicitly excluded in the calculation. Differences arise due to the off-shell properties of these on-shell equivalent potentials. We use the adiabatic hyperspherical method to formulate a practical prescription to exclude Pauli forbidden states in three-body calculations. Schematic as well as realistic potentials are used. Almost indistinguishable results are obtained.

PACS number(s): 21.60.Gx, 21.45.+v

1 Introduction

Cluster models are useful to describe spatially correlated systems when the intrinsic cluster structures essentially are frozen and the relative and intrinsic degrees of freedom essentially are decoupled. A particular application during the last decade has been in studies of nuclear halos [1, 2] and the concepts developed in this connection have already penetrated in to other subfields of physics [3, 4, 5].

When different clusters contain identical particles the Pauli forbidden states must often be excluded. This is conceptually simple but often difficult in practise, since the proper antisymmetrization too easily spoils the advantages of the cluster description. For spatially extended systems with little overlap the details of appropriate approximations have so far been rather unimportant [6, 7, 8, 9, 10, 11]. However, beside the conceptual interest better treatments may be required by the need for higher accuracy.

Furthermore, the validity of the cluster models may be extended to less pronounced halos by an accurate treatment of the exclusion principle. The dilemma is that the cluster models become more accurate with decreasing overlap while the overlap is necessary to provide the interesting structure and the binding energy. Too large an overlap destroys the fundamental decoupling of the intrinsic and relative cluster degrees of freedom, but the exclusion principle becomes important already at a smaller density overlap.

The correlations displayed in two and three-body halos have attracted a lot of interest and in particular those in light nuclei. If the halo consists of one nucleon bound to a nucleus the Pauli forbidden states are easily excluded by precise orthogonalization. However, already three-body systems present more difficulties and approximations are often employed. Various prescriptions have so far been used in numerical calculations on halos consisting of two nucleons and a core [6, 7]. The simplest is to use a nucleon-core effective potential without bound states [8] even when the nucleon then moves in a potential different from that of the identical nucleons within the core. The difference amounts in this way to an additional repulsion accounting for the Pauli exclusion principle.

It is essential that this effective potential reproduces the nucleon-core low-energy scattering properties, i.e. scattering length and effective range or even better the phase shifts as function of energy. Therefore an obvious procedure [12, 13] is to start with a deep potential appropriate for the nucleons in the core. Then construct a phase equivalent, approximate or precise, shallow or repulsive potential [14] and compute the three-body observables of interest. The results could be compared to those obtained with the deep potential and the Pauli forbidden states excluded in one way or another [7, 15].

This procedure must produce two sets of wave functions coinciding at large distances but differing at small distances by the additional node appearing inside the core by use of the deep potential. The idea is therefore that the short-distance behavior must be irrelevant when the cluster model provides a valid description. This conjecture was tested in three-body computations by using two potentials with the same scattering length and effective range [7] and in two-body computations using completely phase equivalent potentials [9].

The purpose of this paper is to investigate the consequences of using completely phase equivalent two-body potentials [9, 12, 13, 14, 15] in three-body calculations based on the adiabatic hyperspherical approach, see e.g. [3, 5]. The method was suggested and previously tested approximately for two neutrons and a core [7]. In this report we shall carefully follow this prescription using phase equivalent potentials and rigorously derive the short and long-distance behavior of the all-decisive effective radial potentials. We shall consider cases when one, two or three of the two-body potentials have Pauli forbidden states characterized by various quantum numbers.

We begin with a brief sketch of the general method in section 2. We then in section 3 give the characteristic properties of the constructed phase equivalent two-body potentials, where we use a simple s -wave potential as an analytical example. In section 4 we derive the short and long-distance properties of the three-body adiabatic effective radial potentials. In section 5 we show a number of qualitatively different numerical examples. Finally section 6 contains a summary and the conclusions.

2 Adiabatic hyperspherical expansion

In the adiabatic hyperspherical method the coordinates of the three-body system are divided into the slow (hyperradius) and fast (angular) variables. The eigenvalues and eigenfunctions for the fast angular degrees of freedom are then calculated for fixed values of the slow radial variable. These eigenfunctions are then used as a basis for expansion of the total wave function. Eigenvalues for the fast angular variables serve as adiabatic potentials for the slow radial variable. The great advantage of this basis is that it correctly reproduces the long-range asymptotic behavior of the three-body systems including the pathological Efimov effect.

2.1 Hyperspherical coordinates

We first introduce the usual Jacobi coordinates [6] for three particles with masses m_i and coordinates \mathbf{r}_i :

$$\mathbf{x}_i = \sqrt{\frac{1}{m} \frac{m_j m_k}{m_j + m_k}} (\mathbf{r}_j - \mathbf{r}_k), \quad \mathbf{y}_i = \sqrt{\frac{1}{m} \frac{m_i(m_j + m_k)}{M}} \left(\mathbf{r}_i - \frac{m_j \mathbf{r}_j + m_k \mathbf{r}_k}{m_j + m_k} \right), \quad (1)$$

where $M = m_1 + m_2 + m_3$ and m is an arbitrary mass scale. The hyperspherical coordinates now consist of a hyperradius $\rho = \sqrt{x_i^2 + y_i^2}$ and five dimensionless angles $\Omega = \{\alpha_i, \Omega_{xi}, \Omega_{yi}\}$, where Ω_{xi} and Ω_{yi} specify each of the directions of \mathbf{x}_i and \mathbf{y}_i and $\alpha_i \equiv \arctan(x_i/y_i)$. The kinetic energy operator T can be written in terms of the hyperspherical coordinates as

$$T = T_\rho + \frac{\hbar^2}{2m\rho^2} \widehat{\Lambda}_\Omega^2, \quad (2)$$

$$T_\rho = -\frac{\hbar^2}{2m} \rho^{-5/2} \frac{\partial^2}{\partial \rho^2} \rho^{5/2} + \frac{15}{4} \frac{\hbar^2}{2m\rho^2}, \quad (3)$$

$$\widehat{\Lambda}_\Omega^2 = -\frac{1}{\sin(2\alpha)} \frac{\partial^2}{\partial \alpha^2} \sin(2\alpha) - 4 + \frac{\widehat{l}_x^2}{\sin^2 \alpha} + \frac{\widehat{l}_y^2}{\cos^2 \alpha}, \quad (4)$$

where \widehat{l}_x^2 and \widehat{l}_y^2 are the angular momentum operators related to the \mathbf{x} and \mathbf{y} coordinates.

2.2 Adiabatic expansion

The three-body hamiltonian is given by

$$H = T_\rho + \frac{\hbar^2}{2m\rho^2} \widehat{\Lambda}_\Omega^2 + \sum_i V_i(\rho, \Omega), \quad (5)$$

where V_i is the interaction between the two particles j and k . Here $\{i, j, k\}$ is a permutation of $\{1, 2, 3\}$. The eigenvalue problem is solved in two steps. First the slow coordinate ρ is fixed and the (always discrete) spectrum $\lambda_n(\rho)$ and the corresponding angular eigenfunctions $\Phi_n(\rho, \Omega)$ are calculated as function of ρ . For this one can either use the Schrödinger equation

$$\left(\widehat{\Lambda}_\Omega^2 + \frac{2m\rho^2}{\hbar^2} \sum_i V_i - \lambda_n(\rho) \right) \Phi_n(\rho, \Omega) = 0, \quad (6)$$

or the equivalent Faddeev equations

$$\left(\widehat{\Lambda}_\Omega^2 - \lambda_n(\rho) \right) \frac{\phi_n^{(i)}(\rho, \Omega)}{\sin(2\alpha_i)} + \frac{2m\rho^2}{\hbar^2} V_i \Phi_n(\rho, \Omega) = 0, \quad i = 1, 2, 3, \quad (7)$$

where the Schrödinger wave function Φ_n is the sum of the Faddeev components $\phi_n^{(i)}$ or more precisely $\Phi_n(\rho, \Omega) = \sum_i \phi_n^{(i)}(\rho, \Omega) / \sin(2\alpha_i)$.

The total wave function $\Psi(\rho, \Omega)$ is expanded on the complete angular basis set Φ_n , i.e.

$$\Psi(\rho, \Omega) = \frac{1}{\rho^{5/2}} \sum_n f_n(\rho) \Phi_n(\rho, \Omega) = \frac{1}{\rho^{5/2}} \sum_{ni} f_n(\rho) \frac{\phi_n^{(i)}(\rho, \Omega)}{\sin(2\alpha_i)}, \quad (8)$$

where the phase space factors $\rho^{-5/2}$ and $[\sin(2\alpha_i)]^{-1}$ for convenience are extracted explicitly.

The radial expansion coefficients $f_n(\rho)$ are then solutions to

$$\begin{aligned} & \left(-\frac{\hbar^2}{2m} \frac{\partial^2}{\partial \rho^2} + \frac{\hbar^2}{2m\rho^2} \left(\lambda_n(\rho) + \frac{15}{4} \right) - Q_{nn}(\rho) + V_3(\rho) - E \right) f_n(\rho) \\ &= \sum_{n' \neq n} \left(-2P_{nn'}(\rho) \frac{\partial}{\partial \rho} - Q_{nn'}(\rho) \right) f_{n'}(\rho), \end{aligned} \quad (9)$$

where $V_3(\rho)$ is an anticipated three-body potential for fine tuning and the coupling terms P and Q are given as

$$P_{nn'}(\rho) = \int d\Omega \Phi_n^*(\rho, \Omega) \frac{\partial}{\partial \rho} \Phi_{n'}(\rho, \Omega), \quad (10)$$

$$Q_{nn'}(\rho) = \int d\Omega \Phi_n^*(\rho, \Omega) \frac{\partial^2}{\partial \rho^2} \Phi_{n'}(\rho, \Omega) \quad (11)$$

with the angular volume element defined by $d\Omega = \sin^2 \alpha \cos^2 \alpha d\alpha d\Omega_x d\Omega_y$. When all but the lowest terms are neglected we obtain the usual adiabatic approximation.

The angular eigenvalues $\lambda_n(\rho)$ are therefore closely related to the adiabatic radial potentials. The behavior of these angular eigenvalues decisively determines the properties of the three-body system. We shall therefore analytically and numerically investigate $\lambda_n(\rho)$ for phase equivalent two-body potentials differing by the number of bound states. We shall especially study the asymptotic properties analytically.

3 Phase equivalent two-body potentials

Let us assume that a two-body system with relative coordinate \mathbf{r} , reduced mass μ and potential V has at least one bound state with the energy $E_{lsj} = -\hbar^2 \kappa^2 / 2\mu$ and the total wave function $\psi_{lsj}(\mathbf{r}) = u_{lsj}(r) r^{-1} \mathcal{Y}_{lsjm}$ expressed in terms of the radial wave function $u_{lsj}(r)$ and the spin-angular part \mathcal{Y}_{lsjm} , where (s, l, j) are the spin, the orbital and total angular momenta, respectively, while m here is the projection of \mathbf{j} on the z -axis. We then construct a new potential

$$V_{pep}(\mathbf{r}) = V(\mathbf{r}) + \Delta V_{lsj}(r), \quad (12)$$

$$\Delta V_{lsj}(r) = -\hat{P}_j \hat{P}_l \hat{P}_s \frac{\hbar^2}{\mu} \frac{d^2}{dr^2} \ln \left(\int_0^r |u_{lsj}(r')|^2 dr' \right), \quad (13)$$

where $(\hat{P}_j, \hat{P}_l, \hat{P}_s)$ are projection operators on states with the corresponding angular momentum quantum numbers. Thus the additional potential $\Delta V_{lsj}(r)$ is an effective radial potential which only is active for the spin and angular momentum quantum numbers of the bound state in question. The potential $V_{pep}(\mathbf{r})$ is only missing the bound state ψ_{lsj} of $V(\mathbf{r})$, but otherwise these two potentials have identical properties, i.e. they are phase equivalent with the same bound state spectrum [9, 12, 13, 14, 15].

If desired this construction can be repeated to eliminate possible other bound states of the new potential. The series of potentials then only differ by the number of bound states.

The wave function $u_{lsj}(r)$ has the following asymptotic forms at short and large distances

$$u_{lsj}(r \rightarrow 0) \propto r^{l+1}, \quad u_{lsj}(r \rightarrow \infty) \propto e^{-\kappa r}. \quad (14)$$

The additional term ΔV_{lsj} in Eq.(12) diverges as r^{-2} at small distances and vanishes exponentially at large distances [9, 12, 13, 14, 15]

$$\Delta V_{lsj}(r \rightarrow 0) \rightarrow \hat{P}_j \hat{P}_l \hat{P}_s \frac{\hbar^2}{\mu} \frac{2l+3}{r^2}, \quad (15)$$

$$\Delta V_{lsj}(r \rightarrow \infty) \rightarrow \widehat{P}_j \widehat{P}_l \widehat{P}_s \frac{4\hbar^2 \kappa^2}{\mu} \exp(-2\kappa r) . \quad (16)$$

We shall in the remaining part of the present paper often consider an original potential V with one bound s -state. This is the most important case in the practical applications for halo states and a generalization is easy and straightforward by use of Eqs.(12) and (13). Properties and procedure can be studied in more details in simple cases. For illustration we therefore construct an analytical s -wave potential and the corresponding solution labeled by “0”. The wave function $u_0(r)$ must be proportional to r at small distances and must fall off exponentially at large distances. One of the simplest functions obeying these constraints is

$$u_0(r) = \sinh(\beta r) \exp(-\alpha r) , \quad (17)$$

which is the solution with the energy E_0 for the potential V_0 given by

$$E_0 = -\frac{\hbar^2}{2\mu}(\alpha - \beta)^2 \equiv -\frac{\hbar^2 \kappa^2}{2\mu} , \quad V_0(r) = \frac{\hbar^2}{2\mu} 2\beta\alpha [1 - \coth(\beta r)] , \quad (18)$$

where $\kappa = \alpha - \beta > 0$.

The asymptotic behavior of this potential is then

$$V_0(r \rightarrow 0) = \frac{\hbar^2}{2\mu} \left(-\frac{2\alpha}{r} + 2\beta\alpha + O(r) \right) , \quad V_0(r \rightarrow \infty) = -\frac{2\hbar^2}{\mu} \beta\alpha \exp(-2\beta r) , \quad (19)$$

where $O(r)$ is a function vanishing at least as fast as r when r decreases towards zero.

The phase equivalent potential in Eq.(12) has the additional term ΔV_0 defined in Eq.(13). For the example in Eqs.(17) and (18) we then get

$$\begin{aligned} \Delta V_0(r) &= \frac{\hbar^2}{\mu} 8\alpha\beta^2(\alpha^2 - \beta^2) \sinh(\beta r) \\ &\times \frac{\alpha(e^{2\alpha r} + 1) \sinh(\beta r) - \beta(e^{2\alpha r} - 1) \cosh(\beta r)}{(\alpha^2(\cosh(2\beta r) - 1) - \beta^2(e^{2\alpha r} - 1) + \alpha\beta \sinh(2\beta r))^2} = \\ &\frac{\hbar^2}{\mu} \frac{16\alpha\beta^2(\alpha^2 - \beta^2)e^{\alpha r} \sinh(\beta r) [\alpha \cosh(\alpha r) \sinh(\beta r) - \beta \sinh(\alpha r) \cosh(\beta r)]}{[\alpha^2(\cosh(2\beta r) - 1) - \beta^2(e^{2\alpha r} - 1) + \alpha\beta \sinh(2\beta r)]^2} , \quad (20) \end{aligned}$$

which only acts on s -waves and asymptotically behaves in agreement with Eqs.(15) and (16).

4 Asymptotics of the angular eigenvalues

The different two-body potentials from section 3 should now be used in the three-body computations described in section 2. Two-body interactions are needed for the three two-body subsystems. Each of these can in principle support Pauli forbidden states of specific but different properties. In any case the angular eigenvalue spectrum, or equivalently the adiabatic radial potentials, is crucial for the behavior of the resulting three-body system. We shall therefore calculate, as far as possible analytically, the leading terms in the asymptotic expansion of the adiabatic radial potentials both for small and large ρ . Numerical examples for all ρ -values are postponed to the next section.

4.1 Short distances

Let us assume that the original two-body potentials are of short range and finite at $r = 0$. The different angular momentum states then decouple in the three-body Schrödinger equation in the small-distance limit $\rho = 0$. For each set of quantum numbers l_x and l_y referring to the i 'th set of Jacobi coordinates, the angular eigenvalue equation in Eq.(6) reduces to

$$\left(-\frac{1}{\sin(2\alpha_i)} \frac{\partial^2}{\partial \alpha^2} \sin(2\alpha_i) + \frac{l_x(l_x+1)}{\sin^2 \alpha_i} + \frac{l_y(l_y+1)}{\cos^2 \alpha_i} + \frac{2m\rho^2}{\hbar^2} \sum_j V_j \right) \Phi_{nl_x l_y} = \nu_n^2 \Phi_{nl_x l_y}, \quad (21)$$

where $\lambda_n = \nu_n^2 - 4$ and the potentials are kept for later use although their contributions vanish for $\rho = 0$. The eigenvalues and the corresponding eigenfunctions are [6, 10, 16]

$$\nu_n = 2(n+1) \quad , \quad n = 0, 1, 2, \dots \quad (22)$$

$$\Phi_{nl_x l_y} = \frac{1}{\sin(2\alpha_i)} P_n^{(l_x+1/2, l_y+1/2)}(\cos 2\alpha_i) Y_{l_x m_x}(\Omega_{xi}) Y_{l_y m_y}(\Omega_{yi}), \quad (23)$$

where Y_{lm} and $P_n^{(l_x+1/2, l_y+1/2)}$ are the spherical harmonics and the associated Legendre polynomials, respectively.

Let us now assume that only one bound state of angular momentum l_x is Pauli forbidden in one of the two-body subsystems, which we choose to relate to the x -coordinate and denote by i . The phase equivalent potential in Eq.(12) then has an additional term ΔV , which for small ρ contributes to Eq.(21) as

$$\frac{2m\rho^2}{\hbar^2} \Delta V \hat{P}_{l_x} \approx \frac{2m\rho^2}{\hbar^2} \frac{(3+2l_x)\hbar^2}{\mu r^2} \hat{P}_{l_x} = \frac{2(3+2l_x)}{\sin^2 \alpha_i} \hat{P}_{l_x}, \quad (24)$$

where we used that $\mu r^2/m = \rho^2 \sin^2 \alpha_i$. All other partial waves remain unchanged.

The Schrödinger equation in Eq.(21) is then for this particular l_x modified at small ρ into

$$\left(-\frac{1}{\sin(2\alpha)} \frac{\partial^2}{\partial \alpha^2} \sin(2\alpha) + \frac{(l_x+2)(l_x+3)}{\sin^2 \alpha} + \frac{l_y(l_y+1)}{\cos^2 \alpha} + \frac{2m\rho^2}{\hbar^2} \sum_j V_j \right) \tilde{\Phi}_{nl_x l_y} = \tilde{\nu}_n^2 \tilde{\Phi}_{nl_x l_y}, \quad (25)$$

where we omitted the index i on the coordinates and tildes indicate the new eigenvalues and eigenfunctions. Thus the Schrödinger equation is changed as if the angular momentum quantum number l_x were increased by two units. For all other partial waves with l_x different from the quantum number of the two-body bound state the Schrödinger equation remains unchanged. The new spectrum and the corresponding eigenfunctions are given by

$$\tilde{\nu}_n = 2(n+2) \quad , \quad n = 0, 1, 2, \dots \quad (26)$$

$$\tilde{\Phi}_{nl_x l_y} = \frac{1}{\sin(2\alpha)} P_n^{(l_x+5/2, l_y+1/2)}(\cos 2\alpha) Y_{l_x m_x}(\Omega_x) Y_{l_y m_y}(\Omega_y). \quad (27)$$

Thus, except for the missing lowest eigenvalue, the three-body angular spectrum for the phase equivalent potential is identical to the original potential up to the first two terms in the expansion for small ρ , i.e.

$$\nu_n^2 = (2(n+1))^2 + \frac{2m\rho^2}{\hbar^2} \sum_i V_i(0) \quad , \quad \tilde{\nu}_n^2 = (2(n+2))^2 + \frac{2m\rho^2}{\hbar^2} \sum_i V_i(0), \quad (28)$$

where $n = 0, 1, 2, \dots$

The next step is to include more than one two-body bound state in the same subsystem. If the orbital angular momenta of these states are different the three-body angular equations decouple and each of them is analogous or identical to Eq.(25). Thus each Pauli forbidden state is removed independently. On the other hand if the angular momenta are equal the procedure for one two-body bound state is repeated and two units have to be added to the corresponding l_x both in Eq.(25) and in the Legendre polynomial of Eq.(27), i.e. $P_n^{(l_x+5/2, l_y+1/2)}$ should be substituted by $P_n^{(l_x+9/2, l_y+1/2)}$ while the spherical harmonics remain unchanged. The spectrum is again identical to that of the original potential except for the missing two lowest eigenvalues.

Let us now assume that more than one of the two-body subsystems have Pauli forbidden states. Using the phase equivalent potentials the three-body Schrödinger equation for small ρ then becomes

$$\left(-\frac{1}{\sin(2\alpha_i)} \frac{\partial^2}{\partial \alpha_i^2} \sin(2\alpha_i) + \frac{\hat{l}_x^2}{\sin^2 \alpha_i} + \frac{\hat{l}_y^2}{\cos^2 \alpha_i} + \sum_j \frac{2(3 + 2l_{xj}^{(0)})}{\sin^2 \alpha_j} \hat{P}_{l_{xj}^{(0)}} + \frac{2m\rho^2}{\hbar^2} \sum_j V_j \right) \tilde{\Phi}_{nL} = \tilde{\nu}_n^2 \tilde{\Phi}_{nL}, \quad (29)$$

where j in the first summation includes subsystems with a Pauli forbidden bound state of angular momentum $l_{xj}^{(0)}$. The projection operator projects on states with the angular momentum $l_x = l_{xj}^{(0)}$ in the j 'th Jacobi coordinate system. When more than one subsystem has a Pauli forbidden state the different partial waves couple already in the limit $\rho = 0$. Therefore we only maintained the conserved total angular momentum L as an index on the solutions.

The spectrum arising from Eq.(29) can not be obtained analytically. Let us then first repeat that treating each of the additional potentials ΔV while neglecting the others results in Eq.(27). Thus simultaneous inclusion of more than one of these potentials related to different subsystems could be expected to move the spectrum by approximately the sum of that obtained by each of the individual treatments. The corresponding approximate wave functions are analogously obtained from Eq.(27) with the appropriate addition of units to the angular momentum quantum numbers in the Legendre polynomials. However, this is not the exact solution due to the coupling of different partial waves. If the states with $l_{x1}^{(0)}$ and $l_{x2}^{(0)}$ are Pauli forbidden in the subsystems labeled “1” and “2”, respectively, all l_{x1} in subsystem “1” couple provided they receive finite contributions from rotation of the state with $l_{x2}^{(0)}$. Thus numerical solutions are required to get the precise solutions.

A better, still approximate, analytically obtained spectrum can be found by first solving the equation when l_{x1} differs from all three $l_{xj}^{(0)}$ and all additional ΔV terms are neglected. The wave functions are then the usual hyperspherical harmonics. Then when l_{x1} equals one and only one of the values $l_{xj}^{(0)}$ we use the wave functions in Eq.(27). When l_{x1} is equal to two or three identical $l_{xj}^{(0)}$ -values the Legendre polynomial in Eq.(27) has to be substituted by $P_n^{(l_x+9/2, l_y+1/2)}$ or $P_n^{(l_x+13/2, l_y+1/2)}$, respectively. The spectrum is finally found approximately by using these approximate wave functions $\tilde{\Phi}_{nl_x l_y}^{(a)}$ and first order perturbation $\Delta E_{nl_x l_y}$ on top of the hyperspherical spectrum where one or more of the lowest levels are missing.

The energy correction is then

$$\Delta E_{nl_x l_y} = \sum_j \langle \tilde{\Phi}_{nl_x l_y}^{(a)} \left| \frac{2(3 + 2l_{xj}^{(0)})}{\sin^2 \alpha_j} \hat{P}_{l_{xj}^{(0)}} - \frac{2(3 + 2l_{xj}^{(0)})}{\sin^2 \alpha_1} \hat{P}_{l_{x1}=l_{xj}^{(0)}} \right| \tilde{\Phi}_{nl_x l_y}^{(a)} \rangle, \quad (30)$$

where again the summation is over the Pauli forbidden states. This means that at most two non-zero terms are present. Unfortunately it is not easier to use this approximation than to compute the spectrum numerically without any approximations.

In conclusion, in the limit of small ρ the original and the phase equivalent potentials have, except for the Pauli forbidden eigenvalues, exactly the same spectrum of angular eigenvalues when all Pauli forbidden states occur in one two-body subsystem. When more than one subsystem support Pauli forbidden states the spectrum is only approximately the same for $\rho = 0$, again excluding the lowest-lying Pauli forbidden levels.

4.2 Large distances

The hyperspherical spectrum is for short-range two-body potentials also obtained in the limit of $\rho = \infty$ as established previously [5, 16, 17, 18]. It is essentially equivalent to the spectrum at $\rho = 0$ given by Eq.(22). However, in addition some of the angular eigenvalues diverge parabolically towards $-\infty$ in a one-to-one correspondence with the bound states in the two-body subsystems. The corresponding wave functions are the hyperspherical harmonics in Eq.(23) except for the lowest diverging levels where the structure at $\rho = \infty$ is that of two particles in a bound state while the third particle is in a continuum state relative to this two-body structure [18].

The convergence towards the hyperspherical spectrum is faster the higher the angular momentum quantum numbers. The limits are reached at distances comparable to the effective ranges of the two-body interactions [5, 10] with the crucial exception of s -waves, where the two-body scattering lengths define the distance for convergence [16]. The different partial waves decouple in the sense that contributions to a given state from higher angular momenta are at least one order smaller in expansions in terms of ρ^{-1} . Thus for example p -waves only receive contributions of the same order in the ρ^{-1} expansion from the s -waves, which in turn only receive contributions of the same order from other s -waves. These couplings are basically determined by the centrifugal barriers increasing with angular momentum.

The relatively fast convergence for the higher angular momentum states isolate the s -waves as the only interesting contributors at large distances. The diverging levels are of special interest, since some of them correspond to Pauli forbidden states, which must disappear by changing to the phase equivalent potentials in Eq.(12). In fact the goal of the present subsection is to compare the three-body angular eigenvalues of deep and phase equivalent two-body potentials differing only by the number of bound states. This should then allow us to design a prescription for removing Pauli forbidden states at large distance.

The necessary subsequent connection from small to large distances requires knowledge of the approach to the asymptotic behavior, i.e. at least a minimum of information about rate of convergence and wave function decomposition during the approach. Here the s -waves are crucial and we shall therefore derive a number of characteristic features at large distances, i.e. corresponding to distances ρ simultaneously outside the effective ranges of all the two-body interactions. These properties are revealed by use of the zero-range potentials with the related analytical solutions.

For short-range potentials and large distances the Faddeev equations are more convenient than the Schrödinger equation. We therefore start with Eq.(7) for s -waves, which means that the partial angular momenta $l_x = l_y = 0$ in all three Jacobi

coordinates. We choose the system labeled i and transform the other two Faddeev components into this system, project out the s -wave components and multiply by $\sin(2\alpha_i)$. The wave function resulting from Φ_n after these operations is denoted by $\Phi_n^{(i)}$ and from Eq.(7) we then obtain the equation of motion as

$$\left(-\frac{\partial^2}{\partial\alpha_i^2} - \nu_n^2\right)\phi_n^{(i)}(\alpha_i) + \frac{2m\rho^2}{\hbar^2}V_i(\sqrt{\frac{\mu_i}{m}}\rho\sin\alpha_i)\Phi_n^{(i)}(\alpha_i) = 0, \quad i = 1, 2, 3, \quad (31)$$

$$\Phi_n^{(i)}(\alpha) = \phi_n^{(i)}(\alpha) + \sum_{j \neq i} \frac{1}{\sin(2\varphi_{ij})} \int_{|\varphi_{ij} - \alpha|}^{\frac{\pi}{2} - |\frac{\pi}{2} - \varphi_{ij} - \alpha|} d\alpha' \phi_n^{(j)}(\alpha'), \quad (32)$$

where $\varphi_{ij} = (-1)^{P(ijk)} \arctan\left(\sqrt{m_k(m_1 + m_2 + m_3)/(m_i m_j)}\right)$ and $P(ijk)$ is the parity of the permutation $\{ijk\}$ while m and $\mu_i = m_j m_k / (m_j + m_k)$ are the normalization mass m and the reduced mass, respectively. The last term in Eq.(32) arises from the transformation of the two Faddeev components different from i , see for example [5, 6, 16]. A complete solution for square well potentials can be found in [16].

For large distances and short-range potentials V_i vanish when α_i is much larger than the largest effective range of the potentials divided by ρ . In this region the free solution is obtained for each Faddeev component $\phi_n^{(i)}$. In the remaining vanishingly small region of α_i -space around $\alpha_i = 0$ the potential V_i contributes. In the region of small α_i the integral in the function $\Phi_n^{(i)}$ in Eq.(32) can be expanded in terms of α_i . To first order we then obtain

$$\Phi_n^{(i)}(\alpha \ll 1) = \phi_n^{(i)}(\alpha) + 2\alpha \sum_{j \neq i} \frac{\phi_n^{(j)}(\varphi_{ij})}{\sin(2\varphi_{ij})}, \quad i = 1, 2, 3. \quad (33)$$

For large distances $\rho \gg R \equiv \max(R_1, R_2, R_3)$, where R_i is the range of the potential V_i , the solution to Eq.(31) in the α_i -region, $x_i \equiv \sqrt{\frac{\mu_i}{m}}\rho\sin\alpha_i > R$, is the free solution

$$\phi^{(j)}(\alpha) = A_j \sin\left[\nu\left(\alpha - \frac{\pi}{2}\right)\right], \quad (34)$$

where A_j is constant. The structure of this solution is by definition independent of the potentials. The wave function $\phi_n^{(j)}(\varphi_{ij})$ in Eq.(33) is then given by Eq.(34), since the argument φ_{ij} is finite.

Increasing the parameter ρ in Eq.(31) effectively decreases the range and increases the strength of the potential and thus the zero-range limit is approached. The related eigenvalue problem can then be reformulated in the limit $\rho \rightarrow \infty$ for zero-range potentials. For $x_i < R_i$ and $\alpha_i \ll 1$ Eq.(31) is approximately given as

$$\left(-\frac{\hbar^2}{2\mu_i} \frac{\partial^2}{\partial x_i^2} - \frac{\hbar^2 \nu_n^2}{2m\rho^2}\right) \phi_n^{(i)}(x_i) + V_i(x_i)\Phi_n^{(i)}(x_i) = 0, \quad i = 1, 2, 3 \quad (35)$$

and for $x_i > R_i$ the potential vanishes. The Schrödinger equation for $\Phi_n^{(i)}$ then arises by adding the three equations in Eq.(35).

The singular points are $\alpha_i = 0$ or $x_i = 0$ and the boundary conditions for these zero-range potentials are then expressed in terms of the two-body scattering lengths a_i as

$$\left[\frac{1}{\Phi_n^{(i)}} \frac{\partial}{\partial x_i} \Phi_n^{(i)}\right]_{x_i=0} = \frac{1}{a_i}, \quad \left[\frac{1}{\Phi_n^{(i)}} \frac{\partial}{\partial \alpha_i} \Phi_n^{(i)}\right]_{\alpha_i=0} = \frac{\rho}{\tilde{a}_i}, \quad i = 1, 2, 3, \quad (36)$$

where we define the modified scattering lengths by $\tilde{a}_i = a_i \sqrt{\mu_i/m}$. Thus in the zero-range limit the eigenvalue spectrum is determined entirely by the scattering lengths

and identical spectra results from potentials with the same scattering lengths. In particular the original deep potential and its phase equivalent partner must then produce identical angular spectra at large distances, where the zero-range limit is reached.

The boundary conditions in Eq.(36) with the explicit expressions for the angular functions in Eqs.(33) and (34) result then in a system of linear equations for the coefficients A_i , i.e.

$$A_i \nu \cos\left(\nu \frac{\pi}{2}\right) + 2 \sum_{j \neq i} \frac{A_j \sin\left[\nu\left(\varphi_{ij} - \frac{\pi}{2}\right)\right]}{\sin(2\varphi_{ij})} = -\frac{\rho}{\tilde{a}_i} A_i \sin\left(\nu \frac{\pi}{2}\right), \quad i = 1, 2, 3. \quad (37)$$

This system of equations has non-trivial solutions only when the corresponding determinant D is zero, i.e. $D \equiv \det\{M_{ij}\} = 0$ with

$$M_{ij} = 2 \frac{\sin\left[\nu\left(\varphi_{ij} - \frac{\pi}{2}\right)\right]}{\sin(2\varphi_{ij})} + \left[\nu \cos\left(\nu \frac{\pi}{2}\right) + \frac{\rho}{\tilde{a}_i} \sin\left(\nu \frac{\pi}{2}\right) \right] \delta_{ij}. \quad (38)$$

When two or three of the scattering lengths are infinitely large $D = 0$ has a specific negative solution ν which results in the so-called Efimov effect [17].

For finite scattering lengths there are two types of solutions to $D = 0$ in the large-distance limit where $\rho \gg \max(|\tilde{a}_i|)$. One type of solution is only present when there is a bound state with binding energy E_b in one of the two-body subsystems j . This is most easily seen if we assume that $\tilde{a}_j < 0$ and $|\tilde{a}_j| \gg R_j$ which imply that the binding energy $E_b \approx \hbar^2/(2\mu_i a_j^2) \equiv \hbar^2/(2m\tilde{a}_j^2)$. Then $D = 0$ has a solution ν which diverges linearly with ρ , i.e.

$$\nu = -i \frac{\rho}{\tilde{a}_i}, \quad \lambda = \nu^2 - 4 \approx -\frac{2m\rho^2}{\hbar^2} E_b. \quad (39)$$

Thus this angular eigenvalue diverges parabolically with ρ at large distance.

The other type of solutions has eigenvalues ν approaching constants as $\rho \rightarrow \infty$. This is understood from the dominance of the terms proportional to ρ in Eq.(38) resulting in the solutions

$$\nu \rightarrow \text{Const}, \quad \sin\left(\nu \frac{\pi}{2}\right) = 0, \quad \nu_n = 2(n+1), \quad n = 0, 1, \dots. \quad (40)$$

displaying a spectrum identical to that obtained for small ρ . These eigenvalues ν can be found to next order in an expansion in powers of ρ by expanding D as

$$\begin{aligned} D = \det\{M_{ij}\} &= \rho^3 \frac{1}{\tilde{a}_1 \tilde{a}_2 \tilde{a}_3} \sin^3\left(\nu \frac{\pi}{2}\right) \\ &+ \rho^2 \left(\frac{\tilde{a}_1 + \tilde{a}_2 + \tilde{a}_3}{\tilde{a}_1 \tilde{a}_2 \tilde{a}_3} \right) \nu \cos\left(\nu \frac{\pi}{2}\right) \sin^2\left(\nu \frac{\pi}{2}\right) + O(\rho), \end{aligned} \quad (41)$$

where $O(\rho)$ at most increases as ρ for $\rho \rightarrow \infty$. These leading two terms then give the eigenvalue equation $D = 0$, i.e.

$$\sin\left(\nu \frac{\pi}{2}\right) + \nu \cos\left(\nu \frac{\pi}{2}\right) \frac{1}{\rho} \sum_i \tilde{a}_i = 0, \quad (42)$$

which has an explicit solution for the inverse function $\rho(\nu)$, i.e.

$$\rho(\nu) = -\frac{\sin\left(\nu \frac{\pi}{2}\right)}{\nu \cos\left(\nu \frac{\pi}{2}\right)} \sum_i \tilde{a}_i. \quad (43)$$

The eigenvalue solutions ν_n to Eq.(42) are then to first order in ρ^{-1} given by

$$\nu_n = 2(n+1) - \frac{4(n+1)}{\pi} \frac{\sum_i \tilde{a}_i}{\rho}, \quad (44)$$

$$\lambda_n = \nu_n^2 - 4 = (2(n+1))^2 - 4 - \frac{16(n+1)^2}{\pi} \frac{\sum_i \tilde{a}_i}{\rho}, \quad (45)$$

where the leading terms already are given in Eq.(40).

In conclusion, the phase equivalent potential has at large distances the eigenvalue spectrum in Eqs.(40) and (45) while the original deep potential has the same spectrum plus the additional eigenvalue in Eq.(39) resulting from the bound state. More two-body bound states would simply result in precisely the same number of parabolically diverging eigenvalues of the form in Eq.(40). Therefore except for this (or these) additional eigenvalue(s) the angular spectra of the two potentials are asymptotically identical in the large-distance limit.

4.3 Connecting small and large-distance eigenvalues

The original and the phase equivalent potentials have identical angular eigenvalue spectra at both large and small distances when only one two-body subsystem has bound states. This agreement includes at least the first two terms in the expansion both for small and large ρ . The deep potential has in a one-to-one correspondence with the two-body bound states in addition a number of low-lying eigenvalues, which diverge parabolically towards $-\infty$ for $\rho \rightarrow \infty$. The structure of the related states is asymptotically precisely that of the bound two-body states with the third particle in the continuum. When more than one two-body subsystem has bound states the small-distance behavior of the two spectra is only approximately identical.

We can now formulate a convincing prescription for dealing with Pauli forbidden states in three-body cluster computations. In complete analogy with the two-body problem, where the lowest eigenvalues of the two-body hamiltonian are forbidden, we declare the lowest angular eigenvalues, or equivalently the lowest adiabatic potentials, as Pauli forbidden. We consequently remove them from the basis for all values of ρ in the subsequent solutions of the radial equations. The resulting spectra for the original potential with the Pauli forbidden states and its phase equivalent partner are then approximately identical for all values of the hyperradius.

The small differences must be compensated by slightly different three-body interactions, see Eq.(9). This adjustment is necessary in any case to ensure that the three-body binding energy is sufficiently precise. Even two-body interactions reproducing the two-body phase shifts would otherwise underestimate the three-body binding energy. The three-body potential is related to polarization of the particles beyond that included already in the two-body potentials. It must then arise when all three particles interact simultaneously, i.e. are close to each other. The three-body potential may also be viewed as an adjustment of the off-shell behavior of the two-body potentials exclusively determined by the on-shell behavior. After the fine tuning practically indistinguishable and almost exactly identical results are obtained by use of the two different two-body potentials with different appropriate three-body potentials.

5 Numerical illustration

The three-body angular eigenvalue spectra are identical or at least approximately identical for short distances for phase equivalent two-body potentials. In addition, the large-distance behavior is determined by the scattering lengths and therefore

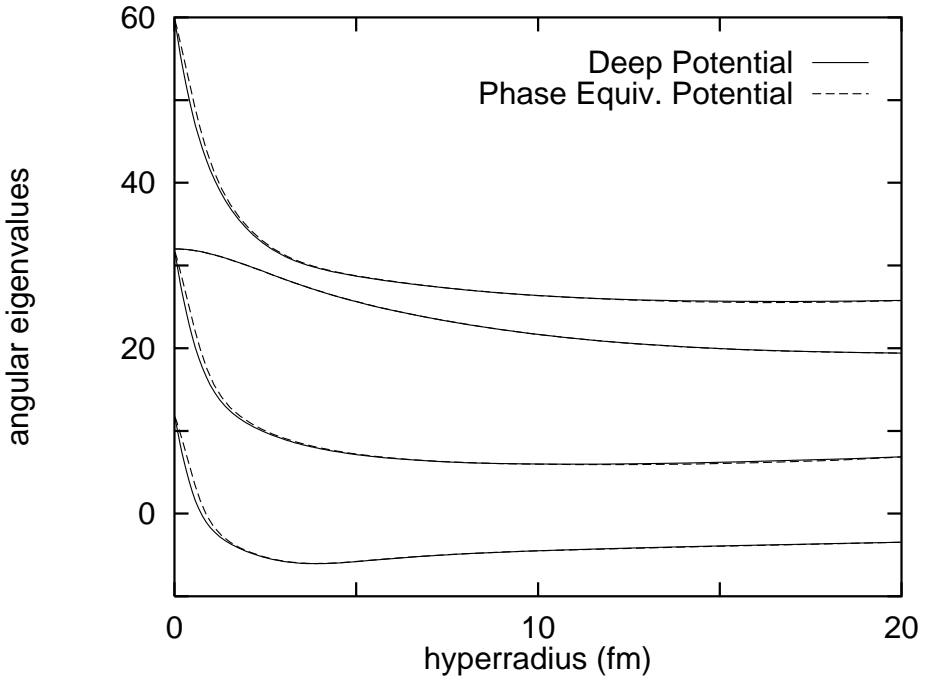


Figure 1: The lowest angular eigenvalues λ_n as functions of hyperradius for the original schematic potential and its phase equivalent partner, see Eqs.(18) and (20). The parameters are $\alpha = 4.151 \text{ fm}^{-1}$ and $\beta = 1.063 \text{ fm}^{-1}$, $\hbar^2/(2\mu) = 41.4 \text{ MeV fm}^2$ and $m_3 = 18\mu$. The other two potentials are equal and given by $V_{13} = V_{23} = -7.8 \text{ MeV} \exp(-(r/2.55\text{fm})^2)$. The lowest parabolically diverging level corresponding to the Pauli forbidden state has been removed. Only s -waves are included in the computation.

also identical for such potentials. The intermediate distances must be studied numerically.

We shall first consider a three-body system where only one two-body subsystem has a bound state. We choose the schematic potentials in Eqs.(18) and (20) for these two particles. The parameters are chosen to reproduce the neutron-neutron scattering length of 18.45 fm and the effective range of 2.83 fm. The two remaining interactions with the third particle are assumed to be equal and given by $V_{13} = V_{23} = -7.8 \text{ MeV} \exp(-(r/2.55\text{fm})^2)$ [8]. The masses correspond to two neutrons and ${}^9\text{Li}$. The three-body system then resembles the halo nucleus ${}^{11}\text{Li}$ (${}^9\text{Li} + \text{n} + \text{n}$) except that now the deep neutron-neutron potential has a bound state.

The resulting lowest angular eigenvalues are shown in Fig. 1 when only s -waves are included in the calculation. The lowest diverging eigenvalue of the original deep potential with the Pauli forbidden state is removed. The two-body potentials behave as r^{-1} at the origin and the eigenvalues are therefore according to Eq.(28) linear functions of ρ for small distances around zero. The hyperspherical spectrum is obtained at large distances. The two spectra are almost indistinguishable for all distances from zero to infinity.

When more than one two-body subsystem has bound states the short-distance behavior of the angular spectra for phase equivalent potentials are only approximately equal. We show in Fig. 2 numerical examples for realistic s -wave potentials for three-body calculations of ${}^9\text{Li} + \text{n} + \text{n}$, where we assume spin-zero for the ${}^9\text{Li}$ -core. With three-body interactions for fine tuning these potentials all produce a

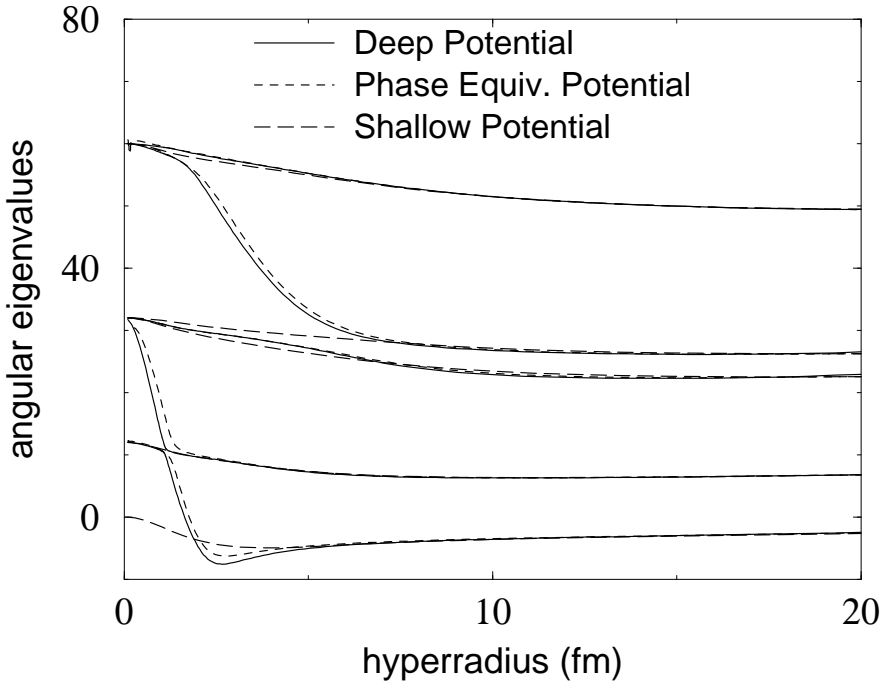


Figure 2: The lowest three-body angular eigenvalues λ_n as functions of hyperradius for realistic s -wave potentials for the ${}^9\text{Li} + \text{n} + \text{n}$ system. The neutron-neutron interaction is from [7]. We use three different neutron- ${}^9\text{Li}$ potential with the same low-energy scattering properties, i.e. (i) a deep potential with Pauli forbidden states, $V_{nc} = -288 \text{ MeV} \exp(-(r/1.15\text{fm})^2)$, (ii) its phase equivalent partner without bound states and (iii) a shallow potential without bound states, $V_{nc} = -5.6 \text{ MeV} \exp(-(r/2.55\text{fm})^2)$ from [11]. Only levels antisymmetric with respect to interchange of the two neutrons are shown. We also removed the lowest parabolically diverging level corresponding to the Pauli forbidden state. Only s -waves are included in the computation.

${}^{11}\text{Li}$ structure in agreement with measurements. By construction the s -wave phase shifts for the deep and phase equivalent potentials are identical for all energies, and indistinguishable from those of the shallow potential for energies below 15 MeV.

The two spectra arising from the truly phase equivalent potentials, (i) and (ii) in Fig. 2, are again almost indistinguishable although they differ slightly more at small and intermediate distances than those in Fig. 1. Otherwise the features of the schematic potential remain for these two potentials. On the other hand the spectrum from potential (iii) differs qualitatively from the other two spectra in spite of the fact that the low-lying s -wave phase shifts are identical for all these three potentials. The hyperspherical spectrum is still for the shallow potential obtained in both limits of $\rho = 0$ and $\rho = \infty$, but now the lowest level starts at $\lambda = 0$ like the (removed) Pauli forbidden level for the deep potential. The phase equivalent potential does not have any level at $\lambda = 0$. The large-distance behavior coincide precisely for all three potentials. The angular eigenvalues are in general more smooth for the shallow potential.

The different behavior at short distance must of course be reflected in different phase shifts at higher energies, but low-energy properties are only marginally influenced. For the same reason the spatially extended halo structure resulting from

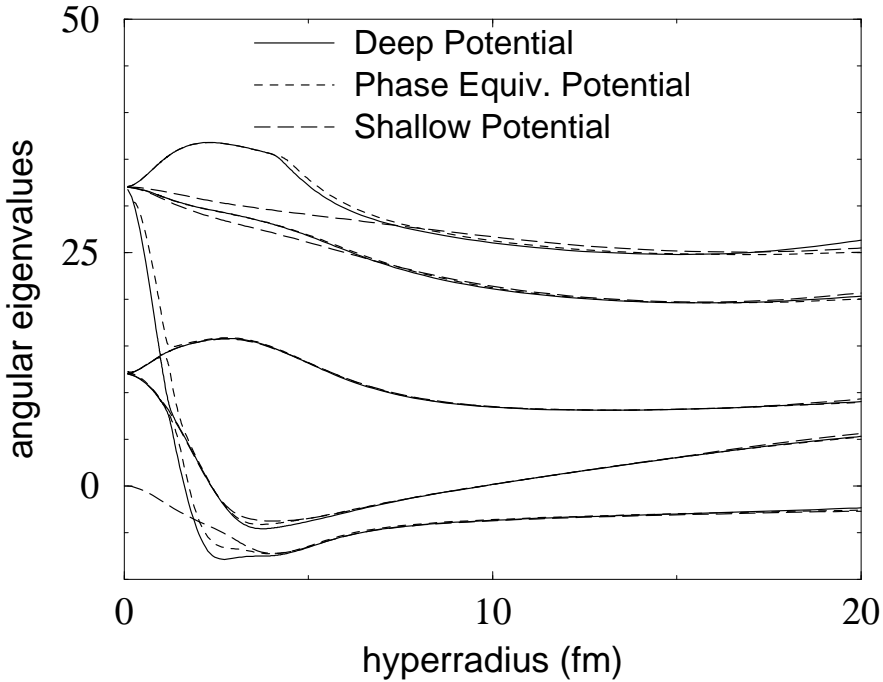


Figure 3: The same as Fig. 2, but now we included both s and p -waves in the neutron- ${}^9\text{Li}$ interaction. The Pauli forbidden states are two-body s -waves and the interactions for s -waves are as in Fig. 2. For p -waves we use the interaction in [11] denoted potential IV, with a central interaction given by $-5.0 \text{ MeV } \exp(-(r/2.55\text{fm})^2)$, and a spin-orbit interaction given by $33.6 \text{ MeV } \mathbf{l}_{nc} \cdot \mathbf{s}_n \exp(-(r/2.55\text{fm})^2)$. These interactions are realistic for use in calculations of halo properties.

these three potentials can hardly be distinguished. This may also be expressed as a dominance of intermediate and large distances in the radial wave function.

The s -wave potentials used in Fig. 2 are realistic choices for computations of the three-body properties of ${}^{11}\text{Li}$. The s -waves are dominating for this system, but the contributions from p -waves are also necessary. These partial waves couple in the three-body computation and several new angular eigenvalues appear as seen in Fig. 3. Comparing to Fig. 2 we can identify the new levels which predominantly are of p -wave character. Even with these couplings the quantitative features of the three potentials are still remarkably similar with the exception of the lowest level for the repulsive s -wave potential.

We also want to compare the spectra when the p -waves dominate in the three-body structure while the Pauli forbidden state still remains in one of the two-body s -wave potentials. A halo nucleus with these features is ${}^6\text{He}$ (${}^4\text{He} + \text{n} + \text{n}$) where the shallow s -wave potential for ${}^{11}\text{Li}$ is substituted by a realistic repulsion. All three potentials (deep, phase equivalent, repulsive) are adjusted to reproduce the measured low-energy s -wave phase shifts. All three angular eigenvalue spectra are shown in Fig. 4 when only s -waves are included.

The repulsion is revealed at small distance by the increasing levels which relatively fast join the corresponding levels from the other two potentials. For the shallow s -wave potential in Fig. 2 the levels from the two phase equivalent potentials varied in contrast relatively fast at small distances, but the outcome is in

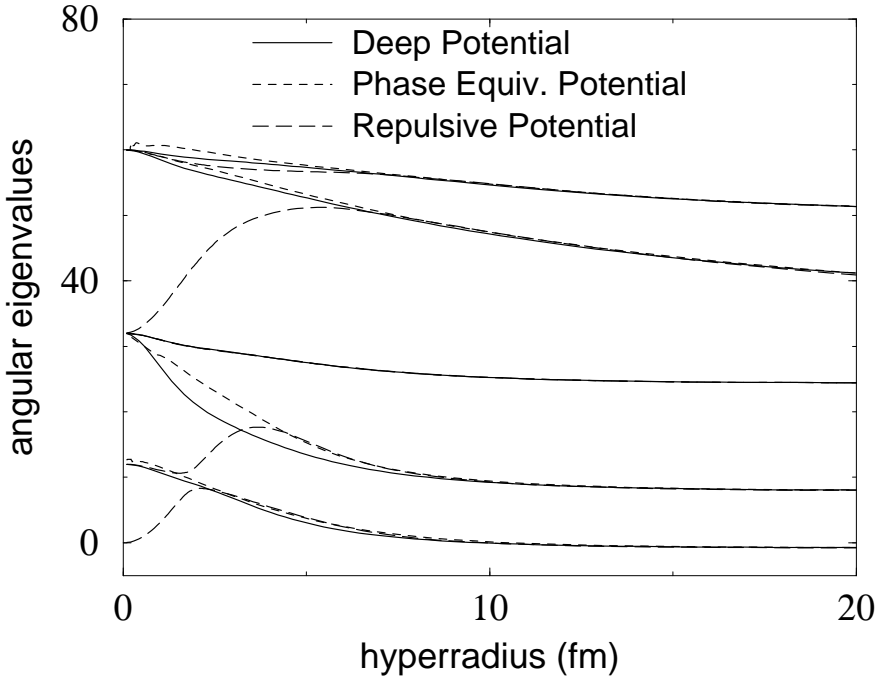


Figure 4: The same as Fig. 2 for the ${}^4\text{He} + \text{n} + \text{n}$ system. The deep potential is given by $-75.06 \text{ MeV} \exp(-r/1.43\text{fm})^2$ and now the shallow potential is substituted by the repulsive potential $48 \text{ MeV} \exp(-r/2.33\text{fm})^2$. The measured low-energy s -wave phase shifts are reproduced by all potentials.

both cases that all spectra quickly becomes very similar and at large distances completely indistinguishable. The overall quantitative agreement between these spectra is again remarkably good.

Including s , p and d -waves in the computation produce more levels and a number of avoided crossings as seen in Fig. 5. However, the larger variation with hyperradius does not spoil the close quantitative resemblance of the three spectra. Instead the agreement is actually improved due to the coupling of the different partial waves and the related avoided crossings. For example the s -wave increasing from the starting point of $\lambda = 32$ on Fig. 4 is now on Fig. 5 quickly joining another level also originating from 32 but with higher angular momentum. Thus, the angular spectra are also remarkably similar when the p -waves dominate as in realistic computations of the three-body properties of the ${}^6\text{He}$ system.

The radial wave function is obtained from Eq.(9) and the lowest is often carrying more than 95 % of the probability. To demonstrate the similarity of the results found by use of the different potentials it is therefore sufficient to show the lowest function f_1 , see Fig. 6. Indeed the quantitative agreement is overwhelming and the curves are essentially indistinguishable except perhaps at the very small hyperradii (blown up and shown in the inset). The slightly smaller probability around the hyperradius of 1 fm for the repulsive potential simply reflects that the effective potential is larger in this region, see Fig. 5. On the other hand the probability is already small and the difference is therefore insignificant. Even these qualitatively different two-body potentials lead to very similar radial wave functions provided the phase shifts are identical. The two phase equivalent potentials produce practically the same radial wave functions for all hyperradii.

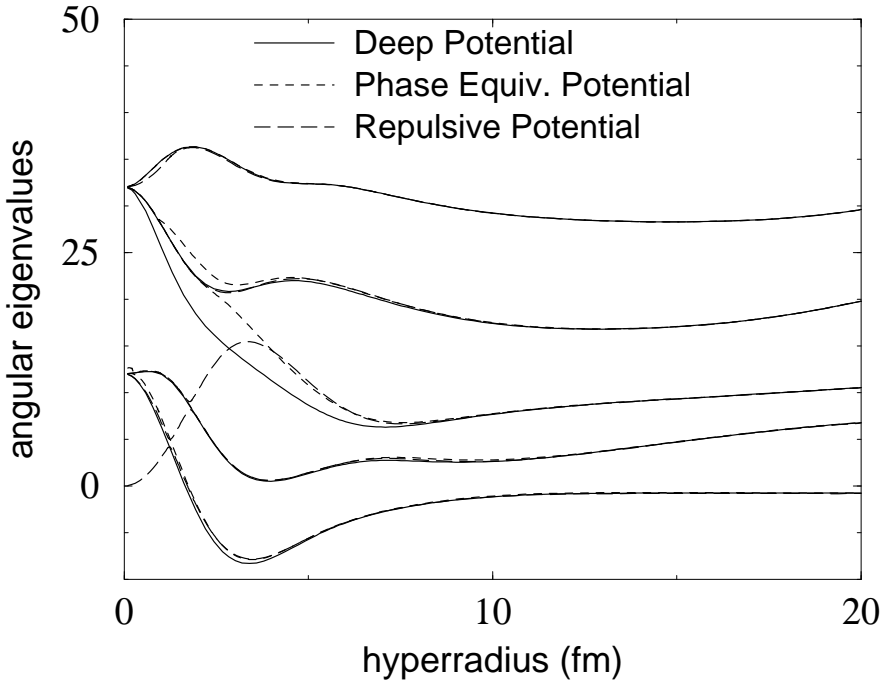


Figure 5: The same as Fig. 4, but now we included both s , p and d -waves. The s -potentials are as in Fig. 4, while the p , d and spin-orbit interactions are taken from [10]. The measured low-energy s -wave phase shifts for all partial waves are reproduced by all potentials. The Pauli forbidden states are two-body s -waves.

6 Summary and conclusion

We use the adiabatic expansion and the hyperspherical coordinates to solve the three-body problem for given short-range two-body potentials. When the three particles are clusters consisting of identical fermions the antisymmetrization between clusters is technically difficult and a number of different practical approximations are used. For nuclear halos the particles are often nucleons interacting with a nucleus. Then this problem can be formulated as exclusion of Pauli forbidden states within the nucleus from the space suspending the physical three-body states. In two-body calculations this is straightforward by direct projection but the use of phase equivalent potentials still provide an interesting alternative.

We use phase equivalent two-body potentials with a different number of bound states and compare the corresponding three-body angular eigenvalue spectra. We show analytically that these spectra, or equivalently the adiabatic radial potentials, at large distances are identical to second order, except for a number of diverging eigenvalues precisely corresponding to the additional Pauli forbidden two-body bound states. This limit is mathematically obtained by use of zero-range potentials and the complete analytical solution is therefore derived and discussed.

We show furthermore analytically that the spectra at small distances, with precisely the same exception for the additional bound states, also are identical to second order provided only one of the two-body potentials differ in the number of bound states. When more than one of the two-body potentials differ in the number of bound states the spectra at small distances are only approximately identical. We give an estimate in perturbation theory of this relatively small deviation.

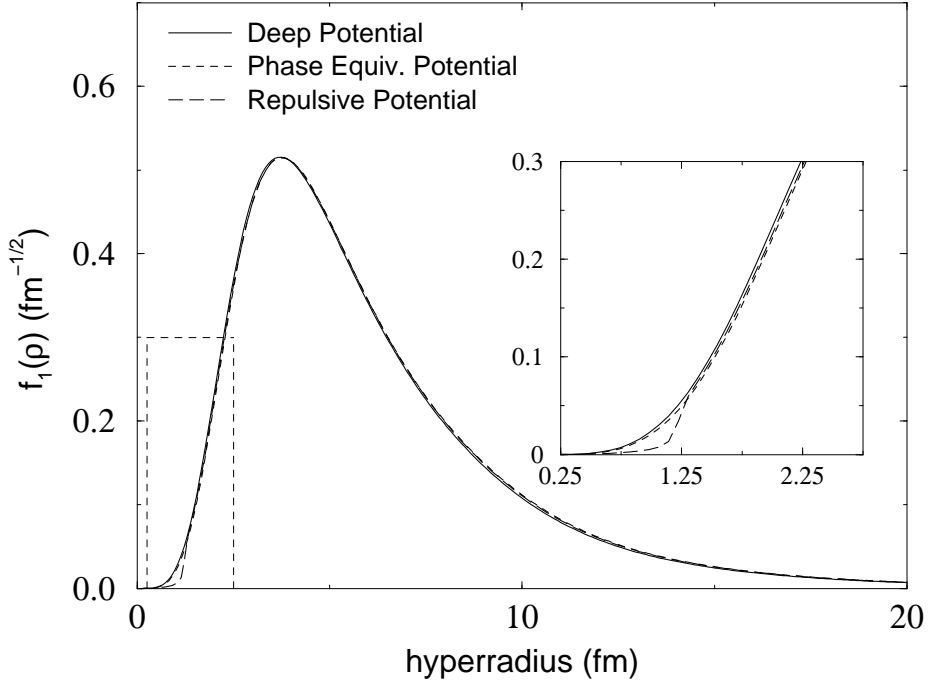


Figure 6: The lowest radial wave function as function of hyperradius for the $^4\text{He} + \text{n} + \text{n}$ system for the potentials used in Fig. 5. The inset shows the small distances where the wave functions differ from zero and that of the repulsive potential from the two other potentials.

In the numerical illustrations we use schematic as well as realistic potentials for the two-neutron halo nuclei ^{11}Li ($^9\text{Li} + \text{n} + \text{n}$) and ^6He ($^4\text{He} + \text{n} + \text{n}$). The bound states are for convenience assumed to be s -states and the two halo nuclei then provide tests on systems where respectively the s and p -configurations dominate in the three-body structure. The three-body angular spectra for phase equivalent potentials are in all cases in remarkable numerical agreement also at intermediate distances. The radial wave function is finally computed for the different potentials. They turn out to be almost indistinguishable for strictly phase equivalent potentials.

However, we find a small difference at very small distances when we use an approximate two-body potential reproducing only the low-energy phase shifts without complete phase equivalence. Such phenomenological potentials have often been used in practical computations of nuclear halo properties. Due to the large spatial extension of halos the probability is by definition very small at small distances and the deviation is therefore insignificant for all practical purposes.

We formulate a prescription to deal with the Pauli principle for two-nucleon halos. Assume that the two-body potentials have Pauli forbidden states. We then construct and use the phase equivalent partners without these forbidden states. The difference between the three-body adiabatic potentials arising from the original and the phase equivalent two-body potentials is essentially only additional basis functions in the hyperspherical adiabatic expansion. Removing these from the adiabatic basis makes the resulting adiabatic spectra asymptotically identical both at small and large distances and approximately equal as well at all the intermediate distances.

The removed basis functions correspond at large distances precisely to two particles in Pauli forbidden states and the third particle in a continuum state. At

small distances the lowest levels of the original deep potentials correspond to identical fermions occupying the same states. Removal of these terms therefore forces the particles to occupy higher-lying orbits and thereby introducing the necessary repulsion preventing violation of the Pauli principle. In conclusion, this method to exclude the Pauli forbidden states in a three-body system has firm mathematical and numerical foundations. It is a practical and accurate alternative to the other existing methods.

References

- [1] P.G. Hansen, A.S. Jensen and B. Jonson, *Ann. Rev. Nucl. Part. Sci.* **45** (1995) 591.
- [2] B. Jonson and K. Riisager, *Phil. Trans. R. Soc. Lond.* **A356** (1998) 2063.
- [3] B.D. Esry, C.D. Lin and C.H. Greene, *Phys. Rev.* **A54** (1996) 394.
- [4] E. Nielsen, D.V. Fedorov and A.S. Jensen, *Phys. Rev.* **A56** (1997) 3287.
- [5] E. Nielsen, D.V. Fedorov and A.S. Jensen, *J. Phys.* **B31** (1998) 4085.
- [6] M.V. Zhukov, B.V. Danilin, D.V. Fedorov, J.M. Bang, I.J. Thompson and J.S. Vaagen, *Phys. Rep.* **231** (1993) 151.
- [7] E. Garrido, D.V. Fedorov and A.S. Jensen, *Nucl. Phys.* **A617** (1997) 153.
- [8] L. Johannsen, A. S. Jensen and P. G. Hansen, *Phys. Lett.* **B244** (1990) 357.
- [9] D. Ridikas, J. S. Vaagen and J. M. Bang, *Nucl. Phys.* **A609** (1996) 21.
- [10] A. Cobis, D.V. Fedorov and A.S. Jensen, *Phys. Rev. Lett.* **79** (1997) 2411; *Phys. Lett.* **B424** (1998) 1; *Phys. Rev.* **C58** (1998) 1403.
- [11] E. Garrido, D.V. Fedorov and A.S. Jensen, *nucl-th/9811016*, *Phys. Rev.* **C** in press.
- [12] A.A. Andrianov, N.V. Borisov and M.V. Ioffe, *Phys. Lett.* **A105** (1984) 19.
- [13] C.V. Sukumar, *J. Phys.* **A18** (1985) 2937.
- [14] D. Baye, *Phys. Rev. Lett.* **58** (1987) 2738.
- [15] H. Fiedeldey, S.A. Sofianos, A. Papastylianatos, K. Amos and L.J. Allen, *Phys. Rev.* **C42** (1990) 411.
- [16] A.S. Jensen, E. Garrido and D.V. Fedorov, *Few-Body Systems* **22** (1997) 1931.
- [17] D. V. Fedorov and A. S. Jensen, *Phys. Rev. Lett.* **71** (1993) 4103.
- [18] D.V. Fedorov, A.S. Jensen and K. Riisager, *Phys. Rev.* **C50** (1994) 2372.